Open Access

Iraqi Journal of Industrial Research (IJOIR)

Journal homepage: http://ijoir.gov.iq

Dynamic Stress Analysis of Turbocharger Blades under High-Velocity Impact Load

[1]Sarah S. Faraj*, [2]Nabil H. Hadi

[1]Renewable Energy and Environment Research Center/ Corporation of Research & Industrial Development, Iraq

[2]Department of Aeronautical Engineering, University of Baghdad, Iraq

Article information

Article history:
Received: June, 12, 2024
Accepted: August, 02, 2024
Available online: December, 14, 2024

Keywords:
Turbocharger,
High-velocity impact load,
Von Mises stress,
Finite Element Model (FEM)

Corresponding Author:
Sarah S. Faraj
s.faraj1803d@coeng.uobaghdad.edu.iq

DOI:
https://doi.org/10.53523/ijoirVol11I3ID485

Abstract

The turbocharger fails due to high pressure and rotational speed. To examine the stress placed on the turbocharger's turbine blade, the analysis focused specifically on the turbine's relation to a 118 kW engine used in automobiles. The turbine operates at a rotational speed of 10000 r.p.m. In calculating the turbine design, factors such as pressure, quantity, breadth, tangential force, mass flow rate, radial force, and the input and output of the blades were considered. The turbine blade design included twelve blades. SolidWorks software was used to study and model the turbine blade of the turbo-engine, and a suitable finite element model was developed. In this project, the turbocharger turbine wheel, with configurations of 8, 10, and 12 blades, was designed and optimized for material selection. When subjected to the same pressure and speed, the Von Mises stress and deformation data were analyzed, comparing aluminum alloys (2618-T61 and 7075-T6), alloy steel, and copper alloys (manganese bronze). The results showed that the turbine wheel experienced minimal Von Mises stress of 175.8 MPa in aluminum alloy (2618-T61) with 12 blades at a ball velocity of 50 m/s, a minimum equivalent elastic strain of 1.503 in alloy steel with 8 blades, and a minimum total deformation of 6.138×10^{-2} mm in alloy steel with 8 blades at a ball velocity of 50 m/s. Therefore, aluminum alloy (2618-T61) with 12 blades was determined to be the most suitable material and configuration for the turbine blade wheel.

1. Introduction

A turbocharger, commonly known as a 'turbo,' is derived from the Greek word "τύρβη" meaning "wake". An air pump called a turbocharger was made to run on the waste energy that ordinarily exists in engine exhaust gas. One type of turbo equipment was the turbocharger. To boost the power of internal combustion engines, the air pressure in the intake must be raised, enabling more fuel to be burned.

The waste energy is used by the turbocharger to compress the air entering the exhaust system, increasing the engine's power by expanding the cylinder. Turbine drives the turbocharging system. Compressed air powered by

exhaust gas (remainder of the gas) in the cylinder. These gasses fuel the turbine shaft and wheel, connected to a compressor wheel that, while in motion, offers large air volume entering the engine's combustion room [1].

The turbine, center housing, and compressor are the three primary components of a turbocharger. The rotating force generated spins the compressor, driven by the exhaust gases passing through the turbine. The air was pulled into the where the compressor housing and wheel were compressed and sent to the recipient via a pipe manifold for engine air intake. Centre -level housing made up of "ball bearings" or "journal" depends on both oil and the application drainage and lubrication. The wind turbine was a piece of turbocharger that receives the engine's exhaust fumes were driven through in order to activate the turbine wheel. A portion of the energy in the hot engine exhaust gas was converted by the turbine into mechanical work, and the temperature and pressure of the amount of exhaust gas drops. Gaseous exhaust from the engine goes into the turbine and runs, executing repairing the turbine seen in Figure (1) [2].

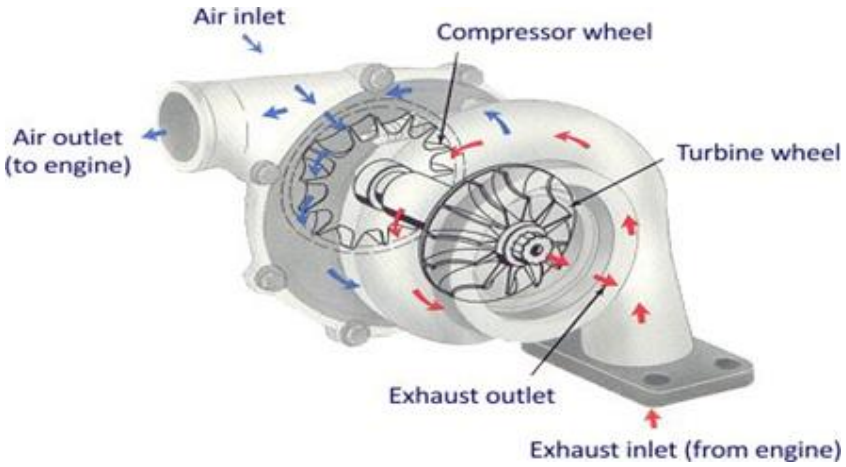

Figure (1): Model showing the working principle of the turbocharger.

The primary distinction between a traditional supercharger and a turbocharger was that the latter was powered by the engine mechanically, which was driven by a turbine powered by the exhaust gas from the engine, in contrast compared to a supercharger with mechanical drive, turbochargers likely to be less responsive yet more efficient [3]. The first exhaust gas turbocharger was completed in 1925 by Alfred Buchi, a Swiss engineer who demonstrated a prototype that boosted a diesel engine's performance by around 40%. The concept of turbo it was not common practice at the time to charge. But over the past few decades, it had evolved into vital in all diesel engines equipped with the exception of little diesel engines. By employing linear analysis, the local peak stresses at the disk root fillet and blade can be reduced. In addition, the corresponding non-linear strain energy was used to determine stress levels and their distribution. The turbine wheel model used in this study was developed, and the Von Mises stresses were analyzed. Ideally, the material selected for turbine wheels in turbochargers should exhibit comparable elastic deformation and strain under identical radial, tangential, and rotational speeds for the three distinct materials tested [4].

Damage had the potential to seriously deteriorate the structure, such a decrease in compressive strength [5]. Impact tests were employed to investigate the failure mechanisms and dynamic deformation of materials. Depending on the impactor's velocity, the material impact can be split into two categories. (i) Low velocity impact (LVI): Tool drops that happen at speeds under 10 m/s cause LVI. (LVI) may be thought of as a quasi-static event, with an upper limit that varies based on the impactor mass and stiffness, target stiffness and material qualities. It can range from one to ten per second. (ii) Intermediate impact this happens at velocities between 10 and 50 m/s. It was caused by debris from hurricanes and tornadoes. (iii) High-velocity (ballistic) impact caused by warhead fragments from explosives or small weapons fire traveling at speeds between 50 and 1000 m/s [6, 7].

The approach for identifying structural deterioration based on alterations in the dynamic properties of the structure was investigated [8]. There were three components to the average impact force. The first section of the test begins at the outset and continues until the impact force reaches it was maximum. Then, because of its

comparatively long duration, the second part (also known as the plateau) begins, during which the majority of the impact energy dissipates. After that, when all of the impact energy was released, the impact force steadily drops until it approaches zero. It's referred to as the unloading portion [9, 10].

The aim of this manuscript is to analyze the structural performance of turbocharger turbine blades under high-velocity impact loads by evaluating stress, strain, and deformation characteristics. Using Finite Element Modeling (FEM) and SolidWorks software, the study examines the effects of different blade configurations (8, 10, and 12 blades) and materials, including aluminum alloys (2618-T61, 7075-T6), alloy steel and copper alloys. The research seeks to identify the optimal blade count and material to enhance the durability and efficiency of turbocharger systems in automotive applications.

2. Impact Load in Turbocharger Blades

When two bodies collide, their surfaces meet at an initial instant known as incidence with a certain relative velocity as shown in Figure (2). Following an incident, there would be interference or penetration of the bodies to increase the pressure at the interface, which develops in the tiny space where two bodies come into touch. This small region is referred to as the impact zone. The pressure in the contact region causes local deformation and ensuing indentation at every moment of the contact period. The impact force is the resultant force of the contact pressure exerted on the two colliding entities in opposite directions at each moment during impact [11].

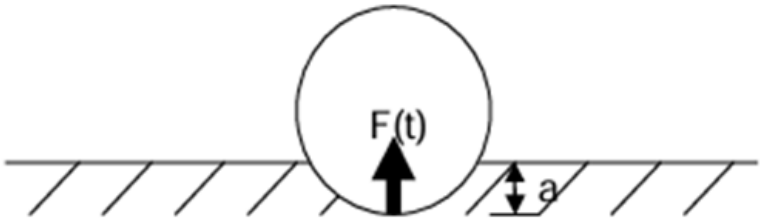

Figure (2): A diagram showing the effect of impact load.

2.1. Kinds of Impact Load

Particle impact, rigid body impact and transverse impact on flexible bodies were the three categories into which impacts may be divided [12].

2.1.1. Impact of Particles

The particle impact approximation just takes into account the normal component of the impact force impulse. The force's source was unknown, although it was likely powerful and had a brief duration; as a result, the impact's duration was only a little instant in time. By taking into account momentum conservation and the law of restitutions, particle impact can offer a fairly straightforward solution when just the impact's kinematics was at stake and the overall structural vibration is minimal.

2.1.2. Rigid Body Impact

When the contact area was small compared to the size of every part, it happens between compact bodies. With an increase in radial distance from the contact zone, the stress created in the contact area decreases quickly. Within a narrow impact zone, the depression is tiny and contained. In addition to the impact kinematics, several contact laws may be used to determine the impact force's temporal history. Rigid body impact can be modeled using massive beam and effective mass models [13].

2.1.3. Transverse Impact on Flexible Bodies

It happens when the collision force causes one of the bodies to flex. As the "stiffness" of the impact zone decreases, the bending lessens the impact force. The vibration caused may result in further collisions. During a collision, one way that energy was lost was through structural vibration. This kind of collision was modelled using the beam vibration model.

2.2. Hertz's Law of Contact

The theoretical analysis of impact, which links the impact force to the local indentation, is based on contact laws. Numerous contact laws with varying characteristics have been established for impacts. The most prevalent of these is Hertz contract law. When there was a collision between hard, compact bodies and the contact zone was tiny, it offers an extremely accurate approximation. The main presumptions of Hertz contact law were as follows:

1. The impactor's spherically shaped surface was in the impact zone.
2. Throughout the hit, the impactor and the beam both maintain their elasticity.
3. During approach and restitution, materials in the impact zone exhibit the same behavior.

Consider a case of a stiff mass striking a beam that was thought to be immobile in the normal direction. Analytical proof shows that, at each point in impact time (t), the impact force (F) was proportional to the 3/2 power of indentation (a) [13].

$$\boldsymbol{F\,(t) = Ka^{3/2}(t)} \qquad \textbf{(1)}$$

The elastic and geometric characteristics of two bodies determine (K), also known as the contact constant. In cases when there was little deformation of the striker in relation to the beam, the contact constant (K) was primarily determined by the striker's radius, the beam's Young modulus and the thickness of the beam [13].

2.3. Massive Impact of Beams

If the mass of the beam was considerably larger than the mass of the striker, the beam impact issue can be greatly simplified. The total velocity of the beam was insignificant in relation to the local deformation at the impact zone.

Assume that the enormous beam was struck by a rigid spherical of mass (m_s)at a velocity of (v_o). The following equation results from the dynamic equilibrium [13].

$$\boldsymbol{F - m_s\ddot{a} = 0} \qquad \textbf{(2)}$$

Hertzian contact law F = $Ka^{3/2}$ may be used to express the above equation as

$$\boldsymbol{Ka^{3/2} - m_s\ddot{a} = 0} \qquad \textbf{(3)}$$

It was possible to get the maximum indentation, maximum impact force and associated time by solving this second order ordinary differential equation as shown in Table (1).

The impact problem's upper bound solution was thought to be found in the large beam model. In this model, in the collision zone, a rigid spherical kinetic energy was transformed into elastic energy. Neglected were the beam's kinetic energy, energy lost via inelastic deformation at the collision zone and structural vibration brought on by the impact.

2.4. Mass Impact Effectiveness

The mass of the beam (m_b) was an additional parameter that the effective mass model adds to the massive beam model. The originally at rest beam was accelerated by the impact force at impact. A rigid sphere and the beam can be compared in terms of relative velocity to model the beam as immobile. In the massive beam model, this was accomplished by lowering the mass of a rigid sphere.

The mass of the rigid sphere (m_s) in the massive beam mode is replaced by virtue of momentum conservation by $\frac{m_s m_e}{m_s+m_e}$ or $\left(\frac{\alpha}{1+\alpha}\right)m_s$ if (α) a mass ratio was the ratio of the rigid sphere mass (m_s) to the effective mass of the beam from the enormous beam impact controlling [13]:

$$F - \left(\frac{\alpha}{1+\alpha}\right) m_s \ddot{a} = 0 \quad (4)$$

3. The Structural Analysis of a Turbine Wheel

Using SolidWorks software, the structural features (Von Mises stress and effective strain) of turbine wheels made from four different materials were investigated and modeled. Figure (3) shows the Turbine Wheel.

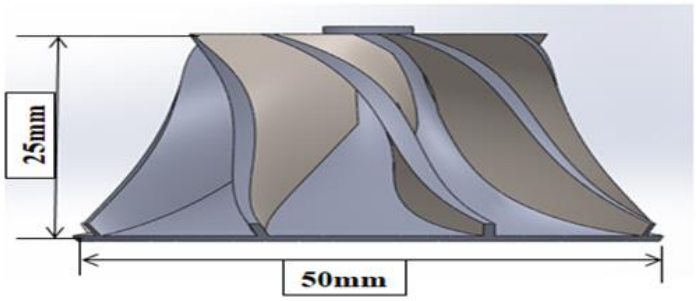

Figure (3): Geometry of turbine wheel with 8 blades.

A high-quality mesh was produced by carefully positioning the generated mesh; boundary condition was then applied to the turbine wheel following the completion of the mesh between the disc that was mounted at the tip of the turbine wheel and the surface of the shaft. The surface of the blades was then subjected to tangential and radial forces, while the surface of the shaft was subjected to rotational speed. Figure (4) depicts mesh and boundary condition model for the turbine wheel.

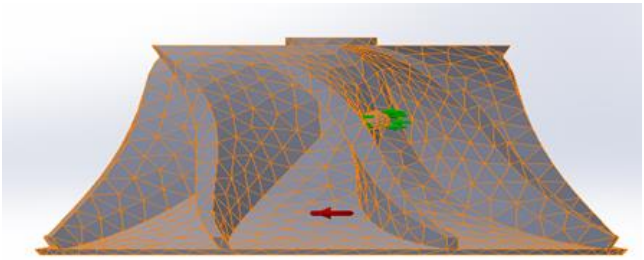

Figure (4): Meshing and boundary condition of turbine wheel with 8 blades.

4. Results and Discussion

4.1. Stress and Displacement Calculations Using FEM

A body's attempt to withstand loads was demonstrated by the development of internal forces, which were generally not constant across different locations. Stress is the measure of internal pressures within a material. Force per unit area was the unit of stress measurement; the word "effective strain" was used in many different contexts, such as particle failure, plastic deformation and ice- structure interaction. It was definition varies according on the situation. Effective strain is often a scalar quantity that indicates the degree of distortion that a material or structure has undergone.

The term "deformation" in engineering describes how an object's size or shape changes. A displacement was the complete shift in a point's location within an item. The relative shift in an object's exterior displacements was known as deflection. A non-dimensional change in the cube's length or angle of distortion can be used to convey strain, which was the relative internal change in form of an incredibly small cube of material. A stress- strain curve connects strains to the forces operating on the cube, sometimes referred to as stress. Up to the yield point, the relationship between stress and strain was often linear, reversible and elastic. Young's modulus was the linear relationship for a material. Plastic deformation was the term used to describe the degree of persistent distortion that persists after unloading over the yield point. The field of material strength and structural analysis may be used to determine the stress and strain distribution within a solid object, using the SolidWork program, obtained the stress, strain and displacement for different materials and different numbers of blades of the turbine wheel, with centrifugal force 10000 r.p.m and velocity of ball 100 m/s as shown in Tables (1, 2, & 3).

4.1.1. Turbocharger with 12 Blades

For the turbine blade wheel with 12 blades and aluminum alloy (2618-T61), Figure (5) shows the Von Mises stress as 3.778×10^{8} N/m², the effective strain as 3.472×10^{-3}, and Figure (6) shows the total deformation as 1.290×10^{-1} mm.

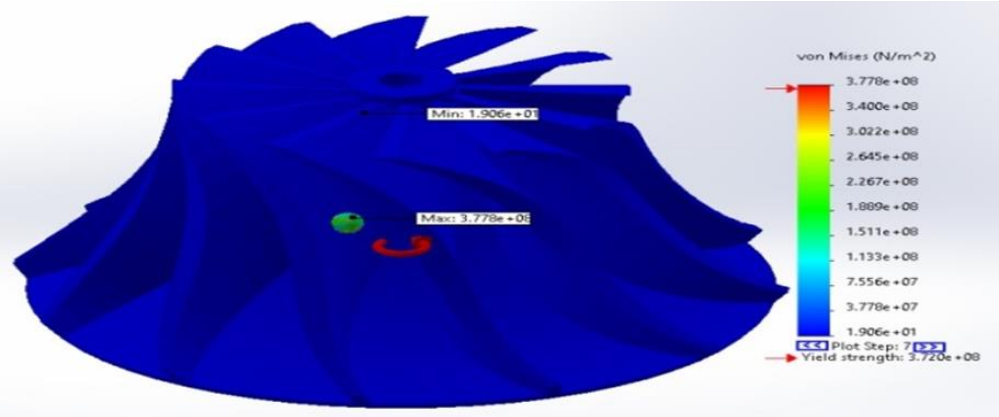

Figure (5): Von-Mises stress on turbine wheel (12 blades) using aluminum alloy (2618-T61).

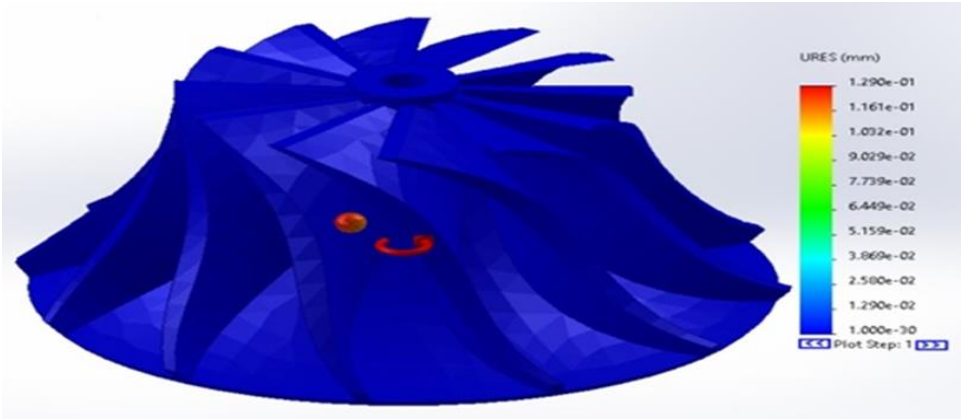

Figure (6): Displacement on turbine wheel (12 blades) using aluminum alloy (2618-T61).

4.1.2. Turbocharger with 10 Blades

For the turbine blade wheel with 10 blades using aluminum alloy (2618-T61), Figure (7) demonstrates that the Von Mises stress is calculated at 3.731×10^{8} N/m², indicating the material's ability to handle substantial loads and rotational forces. This stress level suggests the alloy's resilience under high-pressure conditions, ensuring durability during operation. The effective strain, recorded at 3.216×10^{-3}, reflects the material's deformation under applied stresses. This strain value is within an acceptable range, showing that the alloy can sustain both elastic and minor plastic deformation without failure, critical for applications experiencing cyclical loading.

Figure (8) further illustrates the total deformation, measured at 1.249×10^{-1} mm. This minimal deformation emphasizes the structural stability of the turbine blade under operational conditions, ensuring precise aerodynamic performance and mechanical reliability.

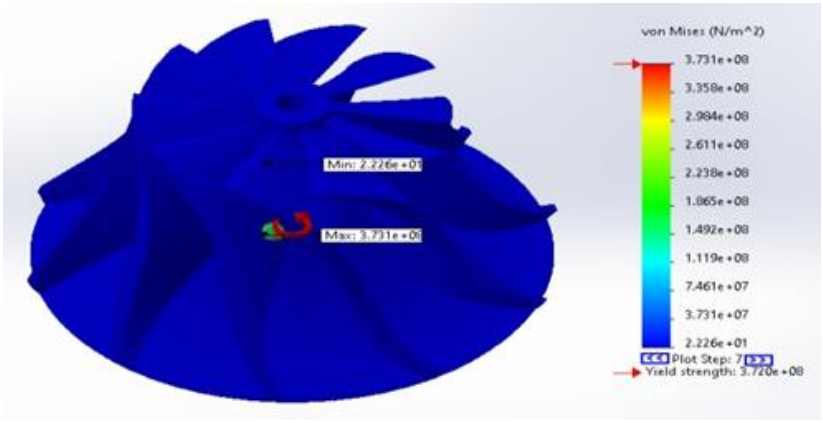

Figure (7): Von-Mises stress on turbine wheel (10 blades) using aluminum alloys (2618-T61).

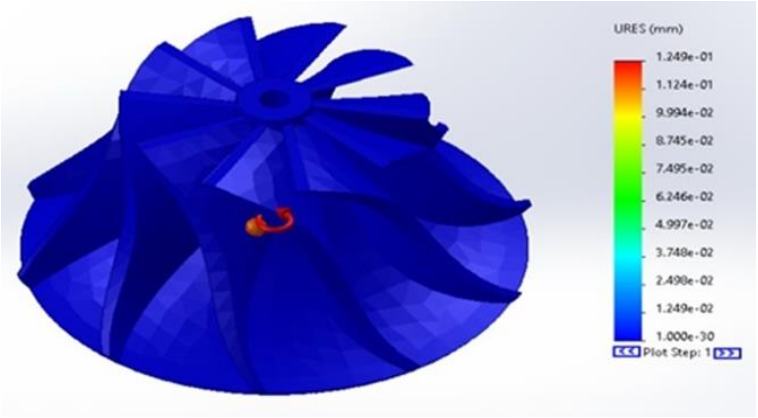

Figure (8): Displacement on turbine wheel (10 blades) using aluminum alloys (2618-T61).

4.1.3. Turbocharger with 8 Blades

For the turbine blade wheel with 8 blades and aluminum alloy (2618-T61), Figure (9) shows the Von Mises stress as 3.824×10^{8} N/m², indicating the stress distribution within the material under operational conditions. The effective strain, measured as 3.155×10^{-3}, reflects the deformation behavior of the material, showing its ability to endure applied forces. Figure (10) displays the total deformation as 1.229×10^{-1} mm, demonstrating the structural stability of the 8-blade configuration under high-speed rotation and load. These results highlight the performance characteristics of this configuration, offering a balance of efficiency and durability for specific applications.

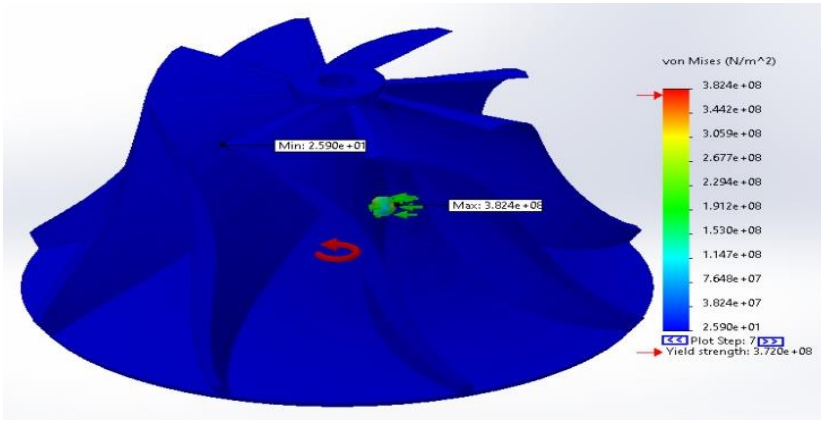

Figure (9): Von Mises stress on turbine wheel (8 blades) using aluminum alloy (2618-T61).

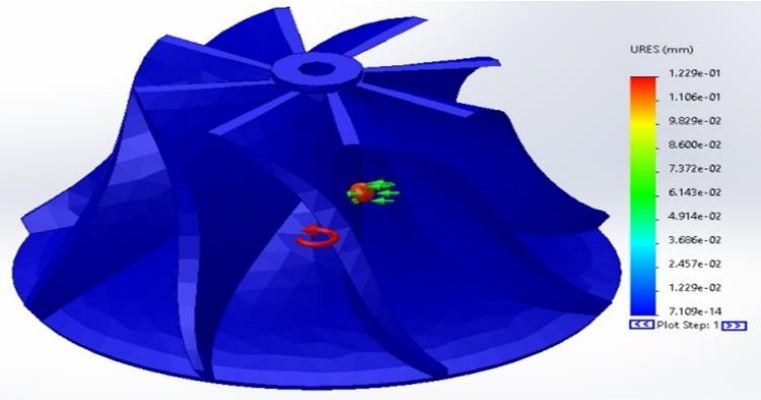

Figure (10): Displacement on turbine wheel (8 blades) using aluminum alloys (2618-T61).

Tables (1, 2, & 3) summery the results of Von Mises stress, effective strain and total deformation for different number of blades, different materials and different velocities.

Table (1): Comparison of Von Mises stress (N/m²) for different turbine wheel materials and ball velocities.

Velocity of ball	Aluminum alloys (2618-T61)		Aluminum alloys (7075-T6)		316 stainless steel		Copper alloys (manganese bronze)	
	Max.	**Min.**	**Max.**	**Min.**	**Max.**	**Min.**	**Max.**	**Min.**
Turbine wheel (12blades)								
100 m/s	3.778×10^{8} (damage)	1.906×10^{1}	6.595×10^{8} (damage)	4.513×10^{2}	1.958×10^{9} (damage)	1.248×10^{3}	9.684×10^{8} (damage)	1.105×10^{3}
75 m/s	2.854×10^{8}	6.898×10^{1}	4.944×10^{8}	4.513×10^{2}	1.468×10^{9} (damage)	1.248×10^{3}	7.267×10^{8} (damage)	1.105×10^{3}
50 m/s	1.758×10^{8}	2.420×10^{2}	3.295×10^{8}	4.513×10^{2}	9.781×10^{8} (damage)	1.248×10^{3}	4.848×10^{8} (damage)	1.105×10^{3}
Turbine wheel (10blades)								
100 m/s	3.731×10^{8} (damage)	2.226×10^{1}	6.553×10^{8} (damage)	4.573×10^{2}	1.921×10^{9} (damage)	1.237×10^{3}	9.662×10^{8} (damage)	1.125×10^{3}
75 m/s	3.568×10^{8}	7.039×10^{1}	4.914×10^{8}	4.573×10^{2}	1.441×10^{9} (damage)	1.237×10^{3}	7.241×10^{8} (damage)	1.125×10^{3}
50 m/s	3.317×10^{8}	4.414×10^{2}	3.275×10^{8}	4.573×10^{2}	9.602×10^{8} (damage)	1.237×10^{3}	4.824×10^{8} (damage)	1.125×10^{3}
Turbine wheel (8blades)								
100 m/s	3.824×10^{8} (damage)	2.590×10^{1}	6.693×10^{8} (damage)	4.138×10^{2}	1.997×10^{9} (damage)	1.134×10^{3}	9.342×10^{8} (damage)	1.015×10^{3}
75 m/s	3.104×10^{8}	6.686×10^{1}	5.022×10^{8}	4.138×10^{2}	1.499×10^{9} (damage)	1.134×10^{3}	7.001×10^{8} (damage)	1.015×10^{3}
50 m/s	3.410×10^{8}	4.169×10^{2}	3.350×10^{8}	4.138×10^{2}	9.997×10^{8} (damage)	1.134×10^{3}	4.664×10^{8} (damage)	1.015×10^{3}

Table (2): Comparison of effective strain for different turbine wheel materials and ball velocities.

Velocity of ball	Aluminum alloys (2618-T61)		Aluminum alloys (7075-T6)		316 stainless steel		Copper alloys (manganese bronze)	
	Max.	Min.	Max.	Min.	Max.	Min.	Max.	Min.
Turbine wheel (12blades)								
100 m/s	3.472×10^{-3}	7.838×10^{-12}	3.648×10^{-3}	7.789×10^{-12}	3.295×10^{-3}	7.528×10^{-12}	7.132×10^{-3}	9.214×10^{-12}
75 m/s	2.603×10^{-3}	7.838×10^{-12}	2.736×10^{-3}	7.789×10^{-12}	2.471×10^{-3}	7.528×10^{-12}	5.348×10^{-3}	9.214×10^{-12}
50 m/s	1.735×10^{-3}	7.838×10^{-12}	1.824×10^{-3}	7.789×10^{-12}	1.647×10^{-3}	7.528×10^{-12}	3.564×10^{-3}	9.214×10^{-12}
Turbine wheel (10blades)								
100 m/s	3.216×10^{-3}	1.050×10^{-11}	3.379×10^{-3}	1.039×10^{-11}	3.052×10^{-3}	9.604×10^{-12}	6.605×10^{-3}	1.382×10^{-11}
75 m/s	2.411×10^{-3}	1.050×10^{-11}	2.534×10^{-3}	1.039×10^{-11}	2.288×10^{-3}	9.604×10^{-12}	4.952×10^{-3}	1.382×10^{-11}
50 m/s	1.607×10^{-3}	1.050×10^{-11}	1.689×10^{-3}	1.039×10^{-11}	1.525×10^{-3}	9.604×10^{-12}	3.300×10^{-3}	1.382×10^{-11}
Turbine wheel (8blades)								
100 m/s	3.155×10^{-3}	9.016×10^{-12}	3.316×10^{-3}	9.367×10^{-12}	3.007×10^{-3}	1.347×10^{-11}	6.466×10^{-3}	1.086×10^{-11}
75 m/s	2.366×10^{-3}	9.016×10^{-12}	2.487×10^{-3}	9.367×10^{-12}	2.255×10^{-3}	1.347×10^{-11}	4.848×10^{-3}	1.086×10^{-11}
50 m/s	1.578×10^{-3}	9.016×10^{-12}	1.658×10^{-3}	9.367×10^{-12}	1.503×10^{-3}	1.347×10^{-11}	3.232×10^{-3}	1.086×10^{-11}

Table (3): Comparison of displacement (mm) for different turbine wheel materials and ball velocities.

Velocity of ball	Aluminum alloys (2618-T61)		Aluminum alloys (7075-T6)		316 stainless steel		Copper alloys (manganese bronze)	
	Max.	Min.	Max.	Min.	Max.	Min.	Max.	Min.
Turbine wheel (12blades)								
100 m/s	1.290×10^{-1}	1.000×10^{-30}	1.292×10^{-1}	4.102×10^{-14}	1.289×10^{-1}	1.153×10^{-13}	1.330×10^{-1}	4.611×10^{-14}
75 m/s	9.674×10^{-2}	1.000×10^{-30}	9.689×10^{-2}	4.102×10^{-14}	9.665×10^{-2}	1.153×10^{-13}	9.976×10^{-2}	4.611×10^{-14}
50 m/s	6.450×10^{-2}	1.000×10^{-30}	6.460×10^{-2}	4.102×10^{-14}	6.444×10^{-2}	1.153×10^{-13}	6.651×10^{-2}	4.611×10^{-14}
Turbine wheel (10blades)								
100 m/s	1.249×10^{-1}	1.000×10^{-30}	1.251×10^{-1}	1.00×10^{-30}	1.248×10^{-1}	1.293×10^{-13}	1.282×10^{-1}	1.408×10^{-13}
75 m/s	9.369×10^{-2}	1.000×10^{-30}	9.380×10^{-2}	1.000×10^{-30}	9.361×10^{-2}	1.293×10^{-13}	9.616×10^{-2}	1.408×10^{-13}
50 m/s	6.246×10^{-2}	1.000×10^{-30}	6.253×10^{-2}	1.000×10^{-30}	6.240×10^{-2}	1.293×10^{-13}	6.410×10^{-2}	1.408×10^{-13}
Turbine wheel (8blades)								
100 m/s	1.229×10^{-1}	7.109×10^{-14}	1.230×10^{-1}	7.813×10^{-13}	1.228×10^{-1}	1.001×10^{-13}	1.262×10^{-1}	1.522×10^{-13}
75 m/s	9.215×10^{-2}	7.064×10^{-14}	9.227×10^{-2}	7.813×10^{-13}	9.207×10^{-2}	1.001×10^{-13}	9.467×10^{-2}	1.522×10^{-13}
50 m/s	6.143×10^{-2}	7.064×10^{-14}	6.152×10^{-2}	7.813×10^{-13}	6.138×10^{-2}	1.001×10^{-13}	6.311×10^{-2}	1.522×10^{-13}

5. Conclusions

The structural analysis of the turbine blade for the turbocharged diesel engine has been addressed in this study work. Three blade configurations (8, 10, and 12) and three mechanical properties—Von Mises stress, effective strain, and total deformation—were analyzed and compared in this study. The yield strength of four distinct materials was more than the maximum Von-Mises stress as obtained. The turbine wheel experiences minimal Von-Mises stress of 175.8MPa in aluminum alloys (2618-T61) with 12 blades at velocity of ball 50 m/s, minimum equivalent elastic strain (1.503) in alloy steel with (8 blades) and minimum total deformation (6.138×10^{-2} mm) in 316 alloy steel with (8 blades), at velocity of ball 50 m/s. The study conducted stress and displacement calculations using FEM to analyse the impact load on turbocharger blades, revealing that internal forces in a body were represented as stress, while deformation refers to the change in size or shape of an object. For turbochargers with different blade counts, the Von Mises stress, effective strain, and total deformation were measured, showing that a 12-blade turbocharger exhibited the lowest Von Mises stress and effective strain compared to 10 and 8 blades. The material comparison highlighted that aluminium alloy (2618-T61) with 12 blades demonstrated the lowest stress and strain, making it the most suitable material for turbocharger applications. These findings suggest that selecting the appropriate material and blade count can significantly enhance turbocharger blade performance and durability, with aluminum alloy (2618-T61) and a 12-blade configuration being particularly effective. Understanding stress and deformation in turbocharger blades is crucial for optimizing design and material selection, emphasizing the importance of material and configuration choices in improving turbocharger efficiency and lifespan.

Conflict of Interest: The authors declare that there are no conflicts of interest associated with this research project. We have no financial or personal relationships that could potentially bias our work or influence the interpretation of the results.

References

[1] M. SAI VASTAV, "Automotive design and analysis of turbo charger with eleven and twelve blades," *International Journal of Mechanical and Production Engineering*, vol. 3, no. 11, pp. 120-125, 2015.

[2] P. Puspitasari, A. Andoko, and P. Kurniawan, "Failure analysis of a gas turbine blade: A review," in *IOP Conference Series: Materials Science and Engineering*, IOP Publishing, p. 12156, 2021.

[3] Y. M. Tereshchenko, E. V. Doroshenko and A. Tehrani, J. Abolhassanzade, "Aerodynamic Factors of Influence on the Resonance Vibration of Gas Turbine Compressor Blades," *Strength Mater*, vol. 47, pp. 711–718, 2015.

[4] M. Akhtar, M. S. Kamran, N. Hayat, A. U. Rehman, and A. A. Khan, "High-vibration diagnosis of gas turbines: An experimental investigation," J. Vib. Control, vol. 27, no. 1–2, pp. 3–17, 2021.

[5] S. Ryu, "Damage detection of composite materials via electrical resistance measurement and IR thermography: A review," 2021.

[6] N. H. Hadi and H. H. Khaleel, "The low-velocity impact response of laminated composite plates with holes," *Journal of Multidisciplinary Engineering Science and Technology*, vol. 2, no.4, pp. 726-733, 2015.

[7] P. Zych and G. Żywica, "Fatigue Analysis of the Microturbine Rotor Disc Made of 7075 Aluminium Alloy Using a New Hybrid Calculation Method," Materials (Basel) 15, 2022.

[8] Erik Dick," Turbocharger Fundamentals", vol. 130, 2022.

[9] M. M. A. Kadhim and A. H. Adheem, "Numerical modelling of CFRP strengthened reinforced concrete beams under impact loading," *Journal of engineering and sustainable development*, vol. xx, no. xx, pp. 1-9, *2018.*

[10] M. V Shitikova, "Fractional operator viscoelastic models in dynamic problems of mechanics of solids: Areview," *Mech. solids, pp. 1–33, 2022.*

[11] C. Baera, H. Szilagyi, C. Mircea and P. Criel, "Concrete structures under impact loading: General aspects," *urbanism arhitectur construcţii*, vol. 7, no. 3, pp. 1-12, 2016.

[12] S. M. Harle, "Exploring the dynamics of vibration and impact loads: a comprehensive review," *Int. J. Struct. Eng.*, vol. 14, no. 1, pp. 1–24, 2024.

[13] I. A. S. Alshaarbaf, E. M. Mouwainea, and A. I. Said, "Numerical analysis of reinforced concrete beams subjected to impact loads," *J. Mech. Behav. Mater.*, vol. 32, no. 1, p. 20220232, 2023.